Sensors & Diagnostics

ROYAL SOCIETY OF CHEMISTRY

PAPER

View Article Online
View Journal | View Issue

Check for updates

Cite this: *Sens. Diagn.*, 2023, **2**, 140

A signal-on electrochemiluminescence immunosensor for A2780 cell detection based on the excellent catalytic performance of Co^{2+} doped TiO_2 nanodisks†

Shupei Zhang,[a] Yitian Huang,[b] Yanjie Chen,[b] Shanshan Yan,[a]
Hong Dai *[ab] and Junhua Zhao[a]

This study aimed at fabricating a new analysis platform for ovarian cancer cells based on metal organic frameworks derived Co^{2+} doped TiO_2 nanodisk (Co-TiO_2 ND) mediated cathodic electrochemiluminescence (ECL) of $Ru(bpy)_3^{2+}$. Concretely, Co-TiO_2 NDs were synthesized by applying a facile strategy and were revealed to possess a mesoporous structure, high surface area, good stability and conductivity, particularly excellent catalytic performance for the oxygen reduction reaction (ORR). Therefore, Co-TiO_2 NDs did not only serve as a promising scaffold to carry amounts of folic acid (FA) for the subsequent immuno-identification reaction but were also utilized to catalyze the ORR reaction and produce substantial $^{\bullet}OH$ to improve the ECL signals of $Ru(bpy)_3^{2+}$. Moreover, helical carbon nanotubes (HCNTs) with strong mechanical strength, excellent electronic transport properties and abundant active sites have emerged as a fascinating sensing matrix for fixing a high quantity of biomolecules (Ab_{CA125}). Then, the target cells A2780 were captured by the specific recognition between Ab_{CA125} and CA125 on A2780 cells, and the FA functionalized probe was attached through the recognition of the FA acceptor on the surface of the cells, which established a "signal on" ECL cytosensor for A2780 detection with a linear range from 2.6×10^2 to 2.6×10^6 cells per mL. Promisingly, the successful application of Co-TiO_2 NDs opens up a new avenue for developing excellent ECL sensors and broadens the application of metal organic frameworks.

Received 23rd August 2022,
Accepted 24th October 2022

DOI: 10.1039/d2sd00148a

rsc.li/sensors

Introduction

Ovarian cancer (OC) as one of the most malignant tumors in females has aroused panic worldwide.[1,2] This is because no palpable symptoms appear until the cancer progresses to advanced stages, which leads to the poor prognosis and high fatality rate.[3,4] Encouragingly, great progress can be made if very early neoplastic changes in the ovarian surface epithelium cells can be detected.[5,6] A2780, an ovarian cancer cell line, was established from an ovarian endometrioid adenocarcinoma tumour in an untreated patient, which is commonly used as a model to observe the effects and test the potency of various chemicals, methods of delivery and treatments for ovarian cancer.[7–9] Therefore, developing an effective technique for A2780 sensitive detection and achieving an early diagnosis of OC is crucial for improving the survival rate of OC patients.

In recent years, many analytical techniques, including cyclic voltammetry (CV),[10] electrochemical impedance spectroscopy (EIS),[11] photoelectrochemistry (PEC),[12] chemiluminescence (CL)[13] and differential pulse voltammetry (DPV),[14] have been proposed to detect tumor cells. However, most of these methods have limited sensitivity for cell analysis. The electrochemiluminescent (ECL) strategy combines the advantages of electrochemistry and CL, which has been applied in many fields owing to its inherent features,[15–17] including good temporal and space controllability, high sensitivity, low-light background and simplicity in operation; enabling the ECL technique can be a promising candidate for cell analysis. Generally, luminophores are required in ECL systems, and tris(2,2-bipyridyl) ruthenium(II) ($Ru(bpy)_3^{2+}$), the most conventional luminophore, has been widely employed because of its high ECL efficiency, excellent water solubility, and good stability.[18] However, many studies have focused on the anodic

---

[a] *College of Chemical and Material Engineering, Quzhou University, Quzhou, Zhejiang, 324000, China. E-mail: luckydai666@163.com*
[b] *College of Chemistry and Chemical Engineering, Fujian Normal University, Fuzhou, Fujian, 350108, China*

† Electronic supplementary information (ESI) available. See DOI: **https://doi.org/10.1039/d2sd00148a**

emission of Ru(bpy)$_3^{2+}$ and rare attention has been paid to its cathodic ECL. Inspired by this knowledge, the cathodic ECL of Ru(bpy)$_3^{2+}$ with tripropylamine (TPrA) as a coreactant was first considered in this study, which is different from the conventional cathodic ECL.[19] Because a strong ECL response is essential to obtain the high sensitivity of the ECL detection,[20,21] some strategies need to be adopted to achieve the amplification of the ECL signal. As proposed by Cao *et al.*, the reactive oxygen species (ROS) generated in the dissolved oxygen reduction reaction (ORR) process can be used to improve the cathodic ECL of Ru(bpy)$_3^{2+}$.[22] Consequently, searching for materials with superior electrocatalytic performance for ORR reactions is urgent.

To date, tremendous efforts have been devoted to exploring efficient ORR catalysts, such as noble metal materials and their alloy nanostructures, which have exhibited charming catalytic properties towards ORR owing to their outstanding electrical conductivity and catalytic activity.[23,24] However, the high cost and poor operational stability limit their extensive application.[25] To overcome this obstacle, alternative catalysts, including carbon materials, non-precious metals and transition metal oxides, have attracted significant interest owing to their distinctive advantages.[26–28] However, carbon material corrosion under harsh electrochemical reaction conditions leads to the loss of electrochemical active surface area and catalytic activity in the long term,[29,30] and the rare surface chemistries and poor biocompatibility of non-precious metals limit their functionalization and biosensing applications.[31] Among the transition metal oxides, TiO_2 is chemically stable, cost-effective, environmentally friendly and easy-functionalization,[32] which may be a good choice in this cytosensing platform. However, the low electronic and ionic conductivity of TiO_2 constrained its application in ORR catalyzing.[33] Consequently, Co^{2+} doped TiO_2 nanodisks (Co-TiO_2 NDs) with mesoporous derived from metal–organic frameworks (MOFs) precursors of MIL-125(Ti)–Co were prepared using a simple method and was revealed to be an efficient ORR catalyst, which remained the initial skeleton of MOFs and displayed promising merits. The unique skeleton structure of MOFs guarantees durability during the ORR process. Moreover, the high porosity, available surface area and excellent conductivity are propitious for exposing active sites and promoting the transfer and transport of electrons and ions, resulting in high ORR activity. More importantly, the rich surface chemistries and good biocompatibility provide great convenience for the loading of biomolecules. Based on these characteristics, the as-prepared Co-TiO_2 NDs are expected to serve as a new probe in the ECL biosensor to remarkably promote the cathodic ECL signal of Ru(bpy)$_3^{2+}$.

To the best of our knowledge, the great steric hindrance and insulation from cells largely inhibit the ECL response.[34] Thus, a proper sensing substrate with admirable conductivity is indispensable in cell analysis. Carbon materials with diverse structures, including carbon nanofibers, carbon nanohorns, carbon nanotubes (CNTs), and grapheme, have become a hotspot in biosensors.[35–37] In particular, helical CNTs (HCNTs), a special three-dimensional helical structure, possess excellent electrical conductivity, large accessible surface area and high mechanical and chemical stability,[38,39] guaranteeing their superiority in cell analysis.

Accordingly, a delicate ovarian cancer cell analysis platform (Scheme 1) was successfully established based on Co-TiO_2 NDs catalytically promoting the cathodic ECL of Ru(bpy)$_3^{2+}$. First, HCNTs with outstanding electron mobility and a large surface area were employed as an efficient sensing matrix to distinctly counteract the hindrance from cells and achieve high loading of Ab_{CA125}. Subsequently, the target cells A2780, Co-TiO_2 NDs@FA were introduced *via* the specific recognition between Ab_{CA125} and CA125 as well as FA and FA acceptor to achieve the fabrication of the ECL biosensor. Interestingly, Co-TiO_2 NDs were first illustrated to be promising catalytically enhanced probe scaffolds. Because of the high efficiency of catalytic performance in the ORR process, Co-TiO_2 NDs trigger intense cathodic emission from Ru(bpy)$_3^{2+}$, which remarkably improves sensitivity for cell analysis. The excellent analytical performance of this sensing platform for A2780 cell detection showed great promise in improving the survival rate of ovarian cancer patients and provided an extensive application to other tumor cell analyses.

Experimental

Material, reagents, apparatus and material preparations

Reagents, apparatus, and the synthesis of HCNTs[40] and Co-TiO_2 NDs[41] were displayed in ESI.†

Synthesis of amino-functionalized HCNTs

Initially, a previously reported strategy[40] was adopted to prepare HCNTs, and *N*,*N*-dimethylformamide was used to disperse the product to obtain a 5 mg mL^{-1} HCNT solution. Subsequently, 100 μL of 5 mg mL^{-1} HCNTs was mixed with 100 μL of 10 mM *p*-phenylenediamine (PPD) and reacted overnight under stirring to complete the π–π stacking reaction between the HCNTs and PPD. After centrifugation and washing with ultrapure water, amino-functionalized HCNTs were acquired and then redispersed in ultrapure water to form a 5 mg mL^{-1} solution for further use.

Preparation of the Co-TiO_2 NDs@FA complex

Primitively, Co-TiO_2 NDs were synthesised based on a previous study[41] with a minor change and then dispersed to form a 2.5 mg mL^{-1} Co-TiO_2 ND solution. Afterwards, 50 μL of 10 mM 3-mercaptopropionic acid (MPA) was mixed with 150 μL of 2.5 mg mL^{-1} Co-TiO_2 ND solution and stirred for 12 h to prepare carboxyl functionalized Co-TiO_2 NDs through the Ti–S bond between the thiol end of MPA and Ti from Co-TiO_2 NDs. After removing the unbounded MPA, the above solution was added to 50 μL of a mixed solution, including 1-ethyl-3-(3-dimethylaminopropyl) carbodiimide hydrochloride (EDC) and

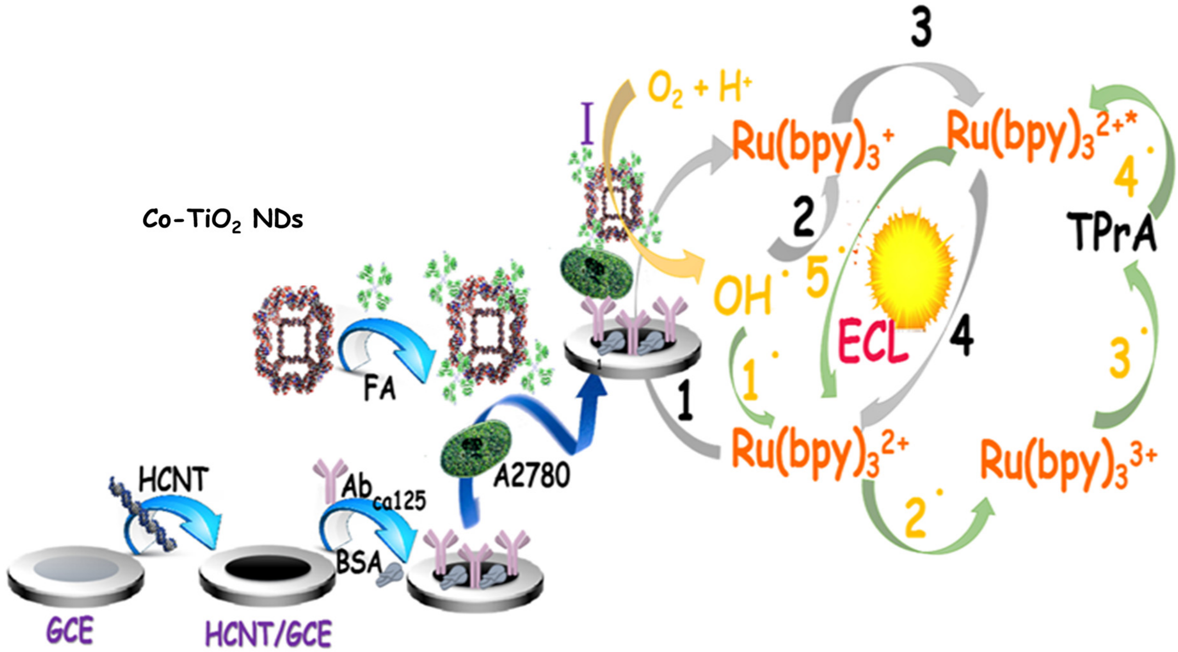

Scheme 1 The fabrication process of this biosensor.

N-hydroxy succinimide (NHS) (molar ratio 4 : 1), to activate the carboxyl groups on the surface of Co-TiO_2 NDs for 1 h at room temperature. Next, 50 μL of 5 mg mL^{-1} FA was placed into it and stirred continuously for 50 min at 37 °C to complete the amide reaction and obtain complexes. Then, the successful preparation was investigated using UV-vis absorption spectra, as demonstrated in Fig. S5.† The obviously decreased but remaining characteristic absorbance peaks of FA can be observed for the Co-TiO_2 NDs@FA hybrids (curve c), which proves the successful formation of the Co-TiO_2 NDs@FA hybrids. Finally, 1.0% bovine serum albumin (BSA) was employed to block the nonspecific binding sites, and the Co-TiO_2 NDs@FA complex was successfully achieved after centrifugation and washing with ultrapure water.

Fabrication of the ECL biosensor

Originally, as described in Scheme 1, the glassy carbon electrode (GCE, Φ = 3 mm) was polished sequentially with 0.3 and 0.05 μm alumina slurry, followed by washing with alcohol and water to obtain a clean surface. Then, 3 μL of 5 mg mL^{-1} HCNT solution was spread on the electrode surface and dried in a drying oven. Subsequently, 10 μL of 2.5% glutaraldehyde (GLD) solution was placed onto the electrode to activate the $-NH_2$ groups of the functional HCNTs for 30 min. Then, the activated electrode was incubated with 10 μL of Ab_{CA125} solution for 30 min at 4 °C. To prevent nonspecific binding sites, 10 μL of 1.0% BSA was dropped on the above electrode for 30 min at 37 °C. Afterwards, the modified electrode was incubated with 50 μL of different concentrations of A2780 cells (with a large amount of CA125 and FA acceptor on the cell surface, as demonstrated in Fig. S1,† by the strep avidin–biotin complex experiment) for 30 min at 37 °C. Ultimately, 10 μL Co-TiO_2 NDs@FA complex was coated on the above electrode and incubated for 30 min at 37 °C to fabricate the ECL biosensor. In each step, the electrode was washed thoroughly with ultrapure water.

ECL measurement

The ECL responses of this biosensor were conducted *via* a three-electrode system in a 2 mL test solution (0.1 M PBS containing 1.0×10^{-5} M $Ru(bpy)_3^{2+}$ and 10 mM TPrA, pH 8.0). The photomultiplier tube voltage was set to 800 V, and the scanning potential ranged from 0 V to −1.6 V (*versus* Ag/AgCl) at a scan rate of 0.05 V s^{-1}. All measurements were carried out using the apparatus described in a previous study.[42]

Results and discussion

Characterization of different materials

To explore the morphologies and microstructures of Co-TiO_2 NDs, the SEM image exhibited a nanodisk structure with a thickness of approximately 100 nm. The rough surface of quasi-disk-shaped Co-TiO_2 NDs with an average size in the range of 200–300 nm can be clearly observed in Fig. 1B, indicating the highly porous structure of Co-TiO_2 NDs. Then, a narrow pore size distribution of around 6 nm can be observed from the N_2 adsorption–desorption isotherm experiments in Fig. S2,† and the results showed that the Co-TiO_2 NDs possessed a large surface area of 178 m^2 g^{-1} and a pore volume of 0.41 cm^3 g^{-1}. In addition, the main characteristic diffraction peaks of (101), (004), and (200) in the XRD pattern (Fig. 1C) were indexed to tetragonal anatase TiO_2 (JCPDS 21-1272). Subsequently, the element distribution

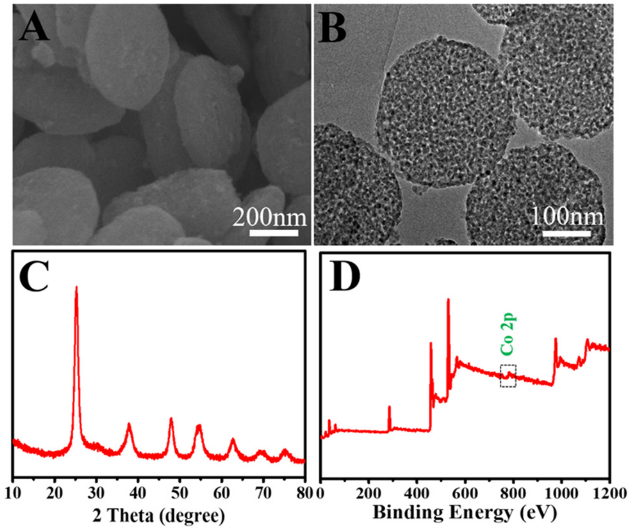

Fig. 1 (A) SEM, (B) TEM image, (C) XRD pattern and (D) XPS analysis of Co-TiO_2 NDs.

of the as-prepared nanodisks was performed (Fig. S3†), and we can observe from the elemental mapping that Co was uniformly doped into the TiO_2 nanodisks and the contents of Co were low. Then, the oxidation states of the chemical compositions were further examined by XPS. As depicted in Fig. 1D, a weak but apparent peak located at 780.1 eV attributed to Co $2p_{3/2}$ was observed, which well agrees with the result in previous studies, verifying that the chemical state of Co^{2+} was successfully doped in Co-TiO_2 NDs. Moreover, the significant peaks at binding energies of 458.4 eV and 464.38 eV belonged to Ti $2p_{3/2}$ and Ti $2p_{1/2}$, respectively, indicating the formation of Ti^{4+}–O bonds. Additionally, the morphology of the HCNTs was examined from the SEM image shown in Fig. S4.† Notably, almost all the HCNTs displayed a high-purity helical structure with a length of 10–40 μm and the diameter could be estimated in the range of 200–400 nm, in which the larger surface provided great convenience for the transfer of electrons and the unique helical structure guaranteed the physicochemical stability of the subsequent signal output.

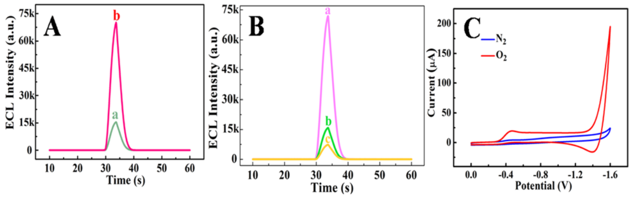

Fig. 2 (A) ECL–time profiles of (a) GCE, (b) Co-TiO_2 NDs/GCE in test solution. (B) ECL responses of Co-TiO_2 NDs/GCE in test solution with bubbling N_2 for (a) 0 minute, (b) 10 minutes and (c) 20 minutes. (C) CV curves of Co-TiO_2 NDs and GCE in 0.1 M KOH solution after bubbling N_2 and O_2 for 30 minutes, respectively.

Exploration of the ECL mechanism

To elucidate the cathodic ECL mechanism of $Ru(bpy)_3{}^{2+}$, the ECL and electrochemical behaviors of various electrodes were investigated. As described in Fig. 2A, the Co-TiO_2 ND modified electrode (curve b) received a rapidly enhanced ECL signal compared with bare GCE (curve a), indicating the importance of Co-TiO_2 NDs in the improvement of the cathodic ECL responses of $Ru(bpy)_3{}^{2+}$. Notably, the ECL signals dropped sequentially with bubbling N_2 from 10 min (curve b) to 20 min (curve c), while the Co-TiO_2 ND modified electrode without bubbling N_2 (curve a) showed the highest ECL signal, as shown in Fig. 2B. These results revealed that oxygen and Co-TiO_2 NDs were essential for the effective emission of cathodic ECL from $Ru(bpy)_3{}^{2+}$. In addition, cyclic voltammetry (CV) was conducted at the Co-TiO_2 ND embellished electrode in different atmospheres. According to Fig. 2C, the Co-TiO_2 ND modified electrode has no reduction peak under N_2, while a significant oxygen reduction peak was observed at −0.45 V under bubbling O_2, which demonstrates that Co-TiO_2 NDs can promote ORR. In combination with previous reports,[42] the possible mechanism of the cathodic ECL of $Ru(bpy)_3{}^{2+}$ in this study is summarized as follows. First, the Co-TiO_2 NDs catalyzed the reduction of dissolved oxygen to release ${}^{\bullet}OH$ (eqn (1)), which further oxidized $Ru(bpy)_3{}^{2+}$ to form $Ru(bpy)_3{}^{3+}$ (eqn (2)). Next, the coreactant TPrA was oxidized to positively charged $TPrA^{+}$ (eqn (3)), which lost a proton to produce the radical TPrA (eqn (4)). $TPrA^{\cdot}$ reacted with $Ru(bpy)_3{}^{3+}$ to generate the excited state of $Ru(bpy)_3{}^{2+}*$ (eqn (5)). In another route, $Ru(bpy)_3{}^{2+}$ accepted an electron to produce $Ru(bpy)_3{}^{+}$ (eqn (6)), which reacted with ${}^{\bullet}OH^{\cdot}$ to form $Ru(bpy)_3{}^{2+}*$ (eqn (7)). Finally, $Ru(bpy)_3{}^{2+}*$ returns to the ground state, emitting ECL (eqn (8)).

$$O_2 + 3H^+ + 4e^- \xrightarrow{\text{Co-TiO}_2\text{NDs}} 2{}^{\bullet}OH + OH^- \tag{1}$$

$$Ru(bpy)_3{}^{2+} + {}^{\bullet}OH \rightarrow Ru(bpy)_3{}^{3+} + OH^- \tag{2}$$

$$Ru(bpy)_3{}^{3+} + TPrA \rightarrow Ru(bpy)_3{}^{2+} + TPrA^{+\bullet} \tag{3}$$

$$TPrA^{+\bullet} \rightarrow TPrA^{\bullet} + H^+ \tag{4}$$

$$Ru(bpy)_3{}^{3+} + TPrA^{\bullet} \rightarrow Ru(bpy)_3{}^{2+}* + TPrA \tag{5}$$

or

$$Ru(bpy)_3{}^{2+} + e^- \rightarrow Ru(bpy)_3{}^{+} \tag{6}$$

$$Ru(bpy)_3{}^{+} + {}^{\bullet}OH \rightarrow Ru(bpy)_3{}^{2+}* + OH^- \tag{7}$$

$$Ru(bpy)_3{}^{2+}* \rightarrow Ru(bpy)_3{}^{2+} + h\nu \tag{8}$$

Excellent electrocatalytic performance of Co-TiO_2 NDs

To evaluate the excellent electrocatalytic activity of Co-TiO_2 NDs during the ORR process, control experiments were

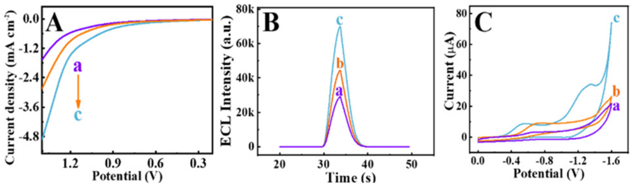

Fig. 3 (A) Polarization curves in 0.1 M KOH solution, (B) ECL responses and (C) CV curves in a test solution of different modified electrodes. (a) P_{25}, (b) TiO_2 MOFs and (c) Co-TiO_2 ND modified electrode.

performed using different materials. First, the polarization curves for commercially available TiO_2 (P_{25}), TiO_2 MOFs and Co-TiO_2 NDs were recorded in Fig. 3A. Significantly, Co-TiO_2 NDs showed the lowest ORR onset potential and highest current density (curve c), reflecting a faster ORR electrocatalytic process than that of TiO_2 MOF (curve b) and P_{25} (curve a). The superior ORR catalytic performance of Co-TiO_2 NDs could be attributed to the doping of Co^{2+}, which increased the oxygen vacancies, resulting in good conductivity.[42] Additionally, to further clarify demonstrate the excellent catalytic performance of Co-TiO_2 NDs, the ECL responses and corresponding CV curves of different material modified electrodes were carried out in test solution. From Fig. 3B, the ECL intensity of the Co-TiO_2 ND modified electrode (curve c) was significantly enhanced compared to those of P_{25} (curve a) and TiO_2 MOF (curve b), which was attributed to the highest catalytic efficiency of Co-TiO_2 NDs for the ORR process. Similarly, as illustrated in Fig. 3C, the oxygen reduction peak shifted positively with the sequential modification of P_{25} (curve a), TiO_2 MOF (curve b) and Co-TiO_2 NDs (curve c). Moreover, the Co-TiO_2 ND decorated electrode presented a higher peak current than the other two materials, which further verifies the excellent electrocatalytic activity of the Co-TiO_2 NDs.

Electrochemical impedance spectroscopy (EIS) and ECL characterization of biosensor construction

To better understand the construction process of this biosensor, the EIS and ECL behaviors were recorded, as depicted in Fig. 4. As demonstrated in Fig. 4A, the GCE decorated with HCNTs (curve b) possessed a smaller impedance value compared with the bare GCE (curve a), which could be explained by the excellent conductivity of the HCNTs in accelerating the diffusion of redox probes to the electrode surface. After successive assembly of Ab_{CA125}, A2780 cells and Co-TiO_2 NDs@FA on the modified electrodes, the impedance values gradually increased (curves c, d and e). This phenomenon was caused by the protein layer, which acted as a blocking layer for mass transfer and greatly hindered electron transport. These results proved the successful fabrication of the ECL biosensor.

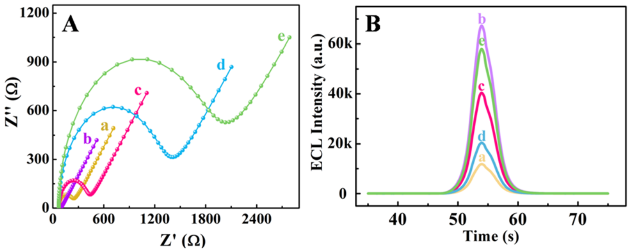

Fig. 4 (A) EIS curves and (B) ECL responses of (a) GCE, (b) HCNTs/GCE, (c) Ab_{CA125}/HCNTs/GCE, (d) A2780 cells (2.6 × 10^3 cells per mL)/Ab_{CA125}/HCNTs/GCE, (e) Co-TiO_2 NDs@FA/A2780 cells/Ab_{CA125}/HCNTs/GCE. The EIS was measured in 0.1 M KCl containing 5.0 mM $[Fe(CN)_6]^{3-/4-}$ and ECL was detected in test solution (0.1 M PBS containing 1.0 × 10^{-5} M $Ru(bpy)_3^{2+}$ and 10 mM TPrA, pH 8.0).

For further clarification of the stepwise assembly process of the electrode, the ECL behaviors were investigated in 0.1 M PBS solution containing 1.0 × 10^{-5} M $Ru(bpy)_3^{2+}$ and 10 mM TPrA. A relatively weak cathodic ECL signal was obtained at the bare GCE (curve a), as shown in Fig. 4B. However, the highest ECL signal was observed after modification with HCNTs (curve b), which served as an effective electron transfer layer, accelerating ECL electron transfer and enhancing ECL emission. Subsequently, the ECL signal declined with the successive incubation of Ab_{CA125} and A2780 cells (curves c and d). This was due to the protein layers that hindered electron transmission. Interestingly, the ECL response was significantly improved after Co-TiO_2 NDs@FA was attached to the above electrode (curve e). The reason for this was that Co-TiO_2 NDs could catalyze the reduction of dissolved oxygen and thus form $^{\bullet}OH$, which played a crucial role in the cathodic ECL emission of $Ru(bpy)_3^{2+}$. Therefore, an efficient ECL strategy was successfully constructed. Based on the above phenomena, with the outstanding catalytic performance of Co-TiO_2 NDs, an efficient ECL sensing platform can be successfully fabricated and used to analyze A2780 cells.

Optimization of experiment conditions

To ensure the high performance of the probe, the concentration of Co-TiO_2 NDs and the reaction time of FA were studied (Fig. S6†). As depicted in Fig. S6A,† the highest cathodic ECL signal for $Ru(bpy)_3^{2+}$ was observed when the concentration of Co-TiO_2 NDs was 2.5 mg mL^{-1}, which was determined as the optimal concentration of Co-TiO_2 NDs. Remarkably, the ECL intensities in Fig. S6B† decreased with the reaction time of FA ranging from 10 to 50 min and then maintained stability. Thus, 50 min was selected as the best reaction time for FA.

Moreover, several influencing factors, including the immobilization time of Ab_{CA125}, A2780 cells, Co-TiO_2 NDs@FA composites, and the pH value of the testing solution, were examined (Fig. S7†). It was clear that the ECL responses gradually decreased as the immobilization time of Ab_{CA125} increased from 10 to 30 min and then reached a plateau (Fig. S7A†). Therefore, 30 min was regarded as the optimum immobilization time for Ab_{CA125}. Similarly, the ECL signal gradually declined until the incubation time of the

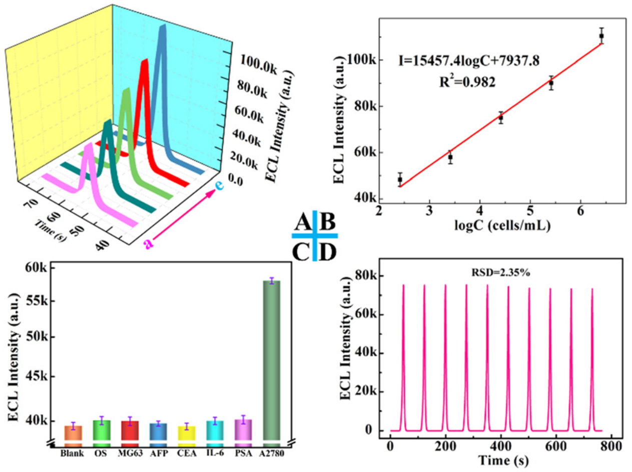

Fig. 5 (A) ECL responses of the proposed ECL biosensor and (B) calibration plot of the ECL intensity with different A2780 concentrations from (a) 2.6 × 10^2 to (e) 2.6 × 10^6 cells per mL in the test solution. (C) The selectivity of the ECL biosensor. (D) The stability of the proposed ECL biosensor (A2780 concentration was 2.6 × 10^4 cells per mL).

A2780 cells was up to 30 min, which can be explained by the electron transfer obstruction resulting from the cells. After 30 min, the ECL intensity remained stable (Fig. S7B†). Thus, the optimal incubation time for A2780 was 30 min. According to Fig. S7C,† the ECL intensity increased as the incubation time of Co-TiO_2 NDs@FA composites increased, and a stable ECL response was achieved at 30 min, which was chosen as the optimal incubation time. Furthermore, the ECL signal reached a peak value at pH 8.0 (Fig. S5D†), so it was selected as the ideal pH value for the detection solution.

A2780 cell determination

Under optimal conditions, the cathodic ECL signals were enhanced as the A2780 cell concentrations increased (Fig. 5A). Moreover, a good linear relationship between the ECL intensity of $Ru(bpy)_3^{2+}$ and the logarithm concentration of A2780 ranging from 2.6 × 10^2 to 2.6 × 10^6 cells per mL was achieved, as illustrated in Fig. 5B. The regression equation is $I = 1.54 \times 10^4 \log C + 7.94 \times 10^3$ (cells per mL) (where I is the ECL intensity of $Ru(bpy)_3^{2+}$ and C is the concentration of A2780) with a correlation coefficient of $R^2 = 0.98$. The result in this study is superior to other cell-based biosensors,[43–45] demonstrating the excellent analytical performance of this cytosensor (Table S1†).

In addition, some interference factors including 10^4 cells per mL OS and MG63 cell, 100 ng mL^{-1} AFP, CEA, IL-6 and PSA antigen were used to examine the selectivity of this proposed sensing platform. As demonstrated in Fig. 5C, compared with the high ECL response of 2.6 × 10^3 cells per mL A2780, the significantly reduced signals were observed from the blank solution and the corresponding interferences, indicating good selectivity. Moreover, a low relative standard deviation (RSD) was achieved under continuous cyclic potential scans for ten cycles (Fig. 5D), indicating the favorable stability of the biosensor. Furthermore, reproducibility was explored as an important factor in estimating the analytical performance of the biosensor. The ECL signals of six electrodes fabricated independently under the same experimental conditions were almost identical (Fig. S8†), and the corresponding RSD was lower than 0.7%, which verified that this biosensor possessed good reproducibility and satisfactory precision.

To evaluate the feasibility of the biosensor for ovarian cancer cell analysis, recovery experiments were conducted using the standard addition method. As can be observed in Table S2,† the recoveries ranged from 96.2 to 107.3% when the blank samples were spiked with different concentrations of A2780 cells, illustrating that the proposed ECL biosensor was viable for A2780 quantitative detection.

Conclusions

In summary, a selective and sensitive A2780 cell analysis platform was established by specific binding between AbCA125 and CA125 on the cell surface as well as FA and its acceptor on the cell surface. Herein, the unique structure and excellent electron mobility of HCNTs enable them to be a desirable sensing matrix to increase the attachment of biomolecules and reduce the electron transfer resistance from cells, thereby improving the cathodic ECL signal of $Ru(bpy)_3^{2+}$. More importantly, highly active electrocatalytic mesoporous Co-TiO_2 NDs that were used as probe nanocarriers to catalyze the ORR process generated a massive $^{\bullet}OH$, which further triggered the strong ECL intensity and achieved high sensitivity in quantitative cell analysis. This ECL sensing strategy holds great promise in early ovarian cancer monitoring and prognosis monitoring and opens up new ideas for other tumour cell analysis.

Conflicts of interest

There are no conflicts to declare.

Acknowledgements

We gratefully acknowledge the financial supports from the National Natural Science Foundation of China (21877012, 21575024), National Science Foundation of Fujian Province (2020J02034, 2019J01052063) and the Health-Education Joint Research Project of Fujian Province (2019-WJ-04).

References

1 K. E. Bairi, O. A. Jarroudi, C. L. Page and S. J. S. i. C. B. Afqir, *Semin. Cancer Biol.*, 2021, **77**, 56–66.
2 A. M. Khalifa, M. A. Elsheikh, A. M. Khalifa and Y. J. J. o. C. R. Elnaggar, *J. Controlled Release*, 2019, **311–312**, 125–137.
3 G. Cammarata, N. Barraco, I. Giusti, V. Gristina, V. Dolo and S. Taverna, *Cancers*, 2022, **14**, 3404–3425.

4 E. Alexandrova, G. Pecoraro, A. Sellitto, V. Melone, C. Ferravante, T. Rocco, A. Guacci, G. Giurato, G. Nassa, F. Rizzo, A. Weisz and R. Tarallo, *Cancers*, 2020, **12**, 1470–1499.

5 R. C. Bast, B. Hennessy and G. B. Mills, *Nat. Rev. Cancer*, 2009, **9**, 415–428.

6 P. E. Colombo, M. Fabbro, C. Theillet, F. Bibeau, P. Rouanet and I. Ray-Coquard, *Crit. Rev. Oncol. Hematol.*, 2014, **89**, 207–216.

7 G. Chiappetta, T. Gamberi, F. Faienza, X. Limaj, S. Rizza, L. Messori, G. Filomeni, A. Modesti and J. Vinh, *Redox Biol.*, 2022, **52**, 102294.

8 B. Nammalwar, R. A. Bunce, K. D. Berlin, D. M. Benbrook and C. Toal, *Eur. J. Med. Chem.*, 2019, **170**, 16–27.

9 Y. Zhang, S. Chang, J. Sun, S. Zhu, C. Pu, Y. Li, Y. Zhu, Z. Wang and R. X. Xu, *Mol. Pharmaceutics*, 2015, **12**, 3137–3145.

10 W. H. Weng, I. L. Ho, C. C. Pang, S. N. Pang, T. M. Pan and W. H. J. B. Leung, *Biosens. Bioelectron.*, 2018, **116**, 51–59.

11 A. R. Correia, I. Sampaio, E. J. Comparetti, N. C. S. Vieira and V. Zucolotto, *Talanta*, 2021, **233**, 122506.

12 R. Y. Li, W. W. Tu, H. S. Wang and Z. H. Dai, *Anal. Chem.*, 2018, **90**, 9403–9409.

13 H. X. Cao, P. F. Liu, L. Wang, Z. J. Liu and G. X. Liang, *Sens. Actuators, B*, 2020, **318**, 128287.

14 X. X. Jian, J. Xu, L. L. Yang, C. X. Zhao, J. W. Xu, Z. D. Gao and Y. Y. Song, *Anal. Chem.*, 2020, **92**, 13319–13326.

15 Y. Cao, J. L. Zhou, Y. W. Ma, Y. Zhou and J. J. Zhu, *Dalton Trans.*, 2022, **51**, 8927–8937.

16 W. Zhao, H. Y. Chen and J. J. Xu, *Chem. Sci.*, 2021, **12**, 5720–5736.

17 Y. T. Fu and Q. Ma, *Nanoscale*, 2020, **12**, 13879–13898.

18 J. Adhikari, M. Rizwan and M. U. Ahmed, *Sens. Diagn.*, 2022, **1**, 878–886.

19 B. Q. Yuan, H. W. Du and T. Y. You, *Talanta*, 2009, **79**, 730–733.

20 R. A. Husain, S. R. Barman, S. Chatterjee, I. Khan and Z. H. Lin, *J. Mater. Chem. B*, 2020, **8**, 3192–3212.

21 M. Saqib, S. Bashir, S. A. Kitte, H. J. Li and Y. D. Jin, *Chem. Commun.*, 2020, **56**, 1827–1830.

22 W. D. Cao, G. B. Xu, Z. L. Zhang and S. J. Dong, *Chem. Commun.*, 2002, 1540–1541.

23 H. Ding, P. Wang, C. J. Su, H. F. Liu, X. L. Tai, N. Zhang, H. F. Lv, Y. Lin, W. S. Chu, X. J. Wu, C. Z. Wu and Y. Xie, *Adv. Mater.*, 2022, **34**, 2109188.

24 K. Maiti, J. Balamurugan, J. Gautam, N. H. Kim and J. H. Lee, *ACS Appl. Mater. Interfaces*, 2018, **10**, 32220–32232.

25 J. J. Duan, S. Chen, S. Dai and S. Z. Qiao, *Adv. Funct. Mater.*, 2014, **24**, 2072–2078.

26 M. M. J. Sadiq, S. Mutyala, J. Mathiyarasu and D. K. Bhat, *J. Electroanal. Chem.*, 2017, 799.

27 N. M. Sanchez-Padilla, D. Morales-Acosta, M. D. Morales-Acosta, S. M. Montemayor and F. J. Rodriguez-Varela, *Int. J. Hydrogen Energy*, 2014, **39**, 16706–16714.

28 L. Zhao, X. L. Sui, J. Z. Li, J. J. Zhang, L. M. Zhang, G. S. Huang and Z. B. Wang, *Appl. Catal., B*, 2018, **231**, 224–233.

29 C. W. Liu, H. S. Chen, C. M. Lai, J. N. Lin, L. D. Tsai and K. W. Wang, *ACS Appl. Mater. Interfaces*, 2014, **6**, 1589–1594.

30 Q. Du, J. Wu and H. Yang, *ACS Catal.*, 2013, **4**, 144–151.

31 C. Hu, J. Qu, Y. Xiao, S. Zhao, H. Chen and L. Dai, *ACS Cent. Sci.*, 2019, **5**, 389–408.

32 T. H. Han, N. Parveen, J. H. Shim, A. T. N. Nguyen, N. Mahato and M. H. Cho, *Ind. Eng. Chem. Res.*, 2018, **57**, 6705–6713.

33 W. Yuan, J. Li, L. Wang, P. Chen, A. Xie and Y. Shen, *ACS Appl. Mater. Interfaces*, 2014, **6**, 21978–21985.

34 L. Gen, M. Cheng, B. K. Jin, Z. X. Chen and J. J. Zhu, *Anal. Chem.*, 2018, **90**, 4801–4806.

35 Z. Y. Wang and Z. H. Dai, *Nanoscale*, 2015, **7**, 6420–6431.

36 R. Eivazzadeh-Keihan, E. B. Noruzi, E. Chidar, M. Jafari, F. Davoodi, A. Kashtiaray, M. G. Gorab, S. M. Hashemi, S. Javanshir, R. A. Cohan, A. Maleki and M. Mahdavi, *Chem. Eng. J.*, 2022, **442**, 136183.

37 J. N. Tiwari, V. Vij, K. C. Kemp and K. S. Kim, *ACS Nano*, 2016, **10**, 46–80.

38 X. Z. Jin, X. D. Qi, Y. Wang, J. H. Yang and Y. Wang, *ACS Appl. Mater. Interfaces*, 2021, **13**, 8808–8822.

39 X. Z. Jin, H. Li, Y. Wang, Z. Y. Yang, X. D. Qi, J. H. Yang and Y. Wang, *ACS Appl. Mater. Interfaces*, 2022, **14**, 27083–27095.

40 Q. Zeng, H. Tian, J. Jiang, X. Ji, D. Gao and C. Wang, *RSC Adv.*, 2017, **7**, 7375–7381.

41 Z. S. Hong, M. L. Kang, X. H. Chen, K. Q. Zhou and M. D. Wei, *ACS Appl. Mater. Interfaces*, 2017, **9**, 32071–32079.

42 J. N. Wang, J. R. Song, H. L. Zheng, X. Q. Zheng, H. Dai, Z. S. Hong and Y. Y. Lin, *Sens. Actuators, B*, 2019, **288**, 80–87.

43 A. Dutta Chowdhury, A. B. Ganganboina, Y. C. Tsai, H. C. Chiu and R. A. Doong, *Anal. Chim. Acta*, 2018, **1027**, 109–120.

44 G. Yang, J. Cao, L. Li, R. K. Rana and J.-J. Zhu, *Carbon*, 2013, **51**, 124–133.

45 R. Li, W. Tu, H. Wang and Z. Dai, *Anal. Chem.*, 2018, **90**, 9403–9409.